

**Fluorometric determination of ornidazole by using BSA coated copper
nanoclusters as a novel turn off sensor**

Mehmetcan BİLKAY^{*}, Hayriye Eda ŞATANA KARA

Department of Analytical Chemistry, Faculty of Pharmacy, Gazi University, Ankara,
Turkey

*Correspondence: mehmetcanbilkay@gazi.edu.tr

ORCID:

Mehmetcan BİLKAY: <https://orcid.org/0000-0003-1625-8666>

Hayriye Eda ŞATANA KARA: <https://orcid.org/0000-0003-1002-9045>

Cite as: Bilkay M, HE Şatana Kara. Fluorometric determination of ornidazole by using BSA coated copper nanoclusters as a novel turn off sensor. Turkish Journal of Chemistry. doi: 10.3906/kim-2109-41

Abstract: A fluorescent probe based on bovine serum albumin stabilized copper nanoclusters (BSA-CuNCs) was developed for the selective and sensitive determination of ornidazole (ORN). The nanoclusters were synthesized via a one-pot hydrothermal process in basic media. The synthesized and characterized BSA-CuNCs have less than 3 nm particle size and exhibited blue emission at 405 nm when excited at 325 nm. Synthesized and characterized nanoclusters were successfully applied as a turn-off fluorescent probe for the determination of ORN in pharmaceutical dosage forms. The quenching mechanism was inner filter effect (IFE). The method was linear in the

concentration range of 0.52-13.56 $\mu\text{g mL}^{-1}$ with a low limit of detection (LOD) 0.01 $\mu\text{g mL}^{-1}$. High recovery values (98.5–102.42 %) with low RSD% values (0.25–2.73%) were obtained. The synthesized nanoclusters can be used as a turn-off probe for ORN determination with their selective, simple, rapid, and inexpensive properties.

Key words: Copper nanocluster, ornidazole, fluorescence sensor, pharmaceuticals

1. Introduction

Ornidazole, ORN, (1-(3-chloro-2-hydroxy)propyl-2-methyl-5-nitroimidazole or 1-chloro-3-(2-methyl-5-nitroimidazole-1-yl)propan-2-ol) is a member of third-generation nitroimidazole [1-3] ORN, which has antiprotozoal and antibacterial properties, shows selective activity against anaerobic, microaerophilic bacteria, and protozoa such as *Trichomonas* and *Entamoeba* species [2,4]. Therefore, it is used in the treatment of infections such as trichomoniasis, amebiasis, and giardiasis, *Helicobacter pylori* duodenal ulcers, metronidazole-resistant strains of *Trichomonas vaginalis*, and also used for prophylaxis in dental and gastric surgery operations [3-5]. Compared to previous nitroimidazoles, ORN has a longer half-life and correspondingly less frequency of dosing. However, the side effects of ORN are mainly nausea, abdominal pain, vomiting, spermatotoxicity, genotoxicity, genomic instability, central nervous system toxicity, and ornidazole-induced autoimmune hepatitis [2]. Analysis of ORN from human plasma, pharmaceutical dosage forms, and other samples have been done with different techniques; these were capillary electrophoresis [4], high performance liquid chromatography (HPLC) used different detectors such as UV [5] and mass spectrometry [6], luminescence spectroscopy [7], and electrochemistry [8]. Although mentioned methods are commonly used and sensitive, they have disadvantages such as

low repeatability, need time-consuming sample preparation steps, high operating cost, and need for expert staff. For this reason, the new sensitive, selective, repeatable, simple applying, time-saving, and cheap method for determination of ORN is needed.

Metal nanoclusters and quantum dots, which are luminescent materials, are very promising compared to organic molecules. However, the use of quantum dots in biological studies can be toxicologically dangerous due to the heavy metals they contain [9, 10]. Metal nanoclusters consisting of several to hundred atoms, they display properties similar to molecules such as spectrochemical and redox properties, magnetism, the HOMO-LUMO transition [11-18]. The most well-known metal nanoclusters (MNCs) are gold (AuNCs) silver (AgNCs) and copper (CuNCs) which are attractive with their size less than 2 nm, on the other hand, the overall size of NCs can be larger with the adding of protective groups to the cluster core [17-20]. Metal nanoclusters have unique features such as low toxicity, quantum-size effect, high photoluminescence efficiency, high Stokes shift, water-solubility, photostability, and easy synthesis procedures. Thus, fluorescent metal nanoclusters are used in a broad applications area in various fields such as sensing, biosensing, ion sensing, bio-labeling, single-molecule imaging, chemical catalysis, and pharmaceutical analysis [11-14]. In these studies, because of the interaction of analyte and nanoclusters, the photoluminescence properties of nanoclusters such as luminescence spectrum and/or lifetime change. Gold, silver, and copper nanoclusters were generally used for their biocompatible features in these studies. Among them, the synthesis of copper nanoclusters is more economical and easier compared to gold and silver nanoclusters [15]. Different synthesis methods are developed to form of nanoclusters based on chemical or photoreduction, chemical etching, ultrasound, and microwave [16]. In these

methods, some of them are using harmful chemicals and needed complicated instruments. Surface ligands not only stabilize NCs but also have a significant effect on their fluorescence properties. Ligands act as a stabilizer that controls the size of NCs, while at the same time altering the surface function of NCs and, accordingly, their fluorescence properties. DNA, proteins, amino acids, peptides, can be used as a template for copper nanoclusters [17]. Recent reports showed that fluorescent copper nanoclusters can be created by proteins from the corresponding metal precursor salt as a precursor. In these studies, bovine serum albumin (BSA), a well-known blood protein, was used forming and stabilizing agent to compose sub-nanosize copper clusters based on reducing of Cu precursors.

In addition, BSA has an important place because it has a strong affinity for inorganic metal ions and small molecules as it contains disulfide bonds and one free cysteine [1]. Besides, the use of BSA as a template also significantly affects the fluorescence properties of CuNCs, which have blue or red emission depending on the synthesis method.

In here, the blue emitting fluorescent BSA capped copper nanoclusters (BSA-CuNCs) were synthesized via a one-pot hydrothermal process without using any organic, strong reducing agents, and additional stabilizers. Synthesized CuNCs were characterized with different methods such as transmission electron microscopy (TEM), infrared spectroscopy (FT-IR), UV-visible (UV-vis), fluorescence, and X-ray photoelectron spectroscopy (XPS), dynamic light scattering analyses (DLS), and zeta potential measurement. In addition, pre-synthesized NCs were used for the determination of ORN in pharmaceutical dosage forms as a turn-off fluorescent probe.

Although there was one study based on using only BSA to determine the ORN [21], in previous studies, the determination of ORN based on interaction with CuNCs in different pharmaceutical forms has not been reported, so, the proposed method has a novelty in this field. The developed method has a low detection limit which indicates the sensitivity of the method, and also is repeatable, fast, simple, inexpensive, and eco-friendly.

2. Experimental

2.1. Chemicals and materials

Ornidazole (ORN), sodium hydroxide, and bovine serum albumin (BSA) were obtained from Sigma–Aldrich Chemical Co. (USA) and used as received without purification. Copper nitrate, phosphoric acid, potassium sulphate, sodium chloride, magnesium chloride, sodium carbonate, potassium nitrate were analytical reagent grades and purchased from Merck (Darmstadt, Germany). The pharmaceutical samples were provided from local pharmacies in Ankara, Turkey. All samples were kept and analyzed at room temperature. Stock ORN solution (1.0×10^{-3} mol L⁻¹) was prepared in deionized water and kept in the refrigerator until analyzing.

Phosphate buffer solutions with different pH (pH 2-11; 0.1 M) and sodium hydroxide solution (0.4 M) were prepared using analytical grade reagents and in deionized water. Sodium hydroxide (5 M) was used to adjust the pH of buffer solutions. Water used throughout was deionized water (>18 MΩ .cm).

2.2. Instrumentation

In order to obtain TEM images, FEI Tecnai G2 Spirit Biotwin CTEM was used. For FT-IR studies Perkin Elmer Spectrum 400 FTIR / FTNIR spectrometer equipped with a Universal ATR Sampling Accessory (Perkin Elmer Inc., Waltham, Ma, USA) was used and spectra were reported in cm^{-1} units. X-ray photoelectron spectroscopic (XPS) analyses were made by using PHI 5000 VersaProbe III multi technique XPS (ULVAC-PHI, Japan). Zeta potential and dynamic light scattering (DLS) analysis were done on a Zetasizer Nano ZS Series, Malvern instrument. UV-Vis spectra were obtained with Specord 50 Plus (Analytik Jena, Germany). Fluorescence measurements were carried out by using the Agilent Cary Eclipse spectrofluorimeter. The excitation wavelength was set at 325 nm and slits were 10.0 nm. Quartz cells with 10×10 mm path length were used for all spectroscopic measurements. pH measurements were done with a Mettler-Toledo GmbH (Greifensee-Switzerland) pH meter. All experiments were carried out at room temperature.

2.3. Synthesis of BSA stabilized CuNCs

Synthesis of BSA stabilized CuNCs were made by minor modification according to the method of Goswami et al [22]. Briefly, 1 ml, 20 mM aqueous $\text{Cu}(\text{NO}_3)_2 \cdot 3\text{H}_2\text{O}$ was taken into the beaker. Then 5 mL, 15 mg/mL BSA solution was added to this solution and stirred for 3 minutes at room temperature. After the mixing step, pH was adjusted to 12 by adding NaOH. Upon reaching pH 12, the color of the solution changed from pale green to purple. Finally, the mixture was stirred vigorously at 55°C for 7 hours. After that time the color of the solution changes to light brown. Synthesized nanoclusters were stored in the refrigerator.

2.4. Analysis of pharmaceutical dosage forms

In this study, ORN was determined in different pharmaceutical dosage forms such as tablets and injection forms.

To prepare tablet samples, ten tablets containing ORN were weighed and powdered finely in a mortar. An appropriate amount of powder was weighed accurately, taken into the volumetric flask, and diluted with deionized water. Then it was sonicated for 30 minutes and centrifuged for 10 minutes. The obtained supernatant was used for the measurements.

In order to prepare the injection form sample, 20 μ l of the sample was taken and completed with 10 ml of deionized water in the flask, then vortexed for one minute.

2.5. Interaction between ORN and BSA stabilized copper nanoclusters

Before interaction studies, the effect of pH on ORN and BSA-CuNCs was examined. For this purpose phosphate buffer solutions at different pH (pH 2-12; 0.1 M) and 0.1 M NaOH solution (pH 13) values were tested.

In order to evaluate of interaction between ORN and BSA-CuNCs, a 2.0 mL 0.1 M pH 12 phosphate buffer solution containing an appropriate concentration of BSA-CuNCs was added into the quartz fluorescence cell, and then it was titrated by successive additions of a stock solution of ORN. Titration was done by using a micropipette manually. The fluorescence emission spectra were recorded in the wavelength range of 335-500 nm with an exciting wavelength at 325 nm in the presence and absence of ORN.

The fluorescence intensity changing of nanoclusters as a result of interaction was determined using the ratio of fluorescence intensities of CuNCs in the absence (F_0) and the presence of ORN (F). All measurements were done with three replicates and for the calculations obtained average values were used.

2.5. Selectivity studies

In order to evaluate possible interference coming from excipients in pharmaceutical dosage forms and the selectivity of the proposed method selectivity studies were done. For this purpose, the effect of some possible commonly interfering ions such as potassium, sodium, magnesium, chloride, sulphate, carbonate, nitrate, and excipients such as propylene glycol and ethanol in injection form, starch and magnesium stearate in tablets on the fluorescence emission intensity of BSA-CuNCs was examined. In this study, the concentrations of ORN and interferents were 36 μM and 360 μM , respectively. The fluorescence emission values of nanoclusters were recorded by adding both ORN and interfering ions/molecules separately on BSA-CuNCs.

3. Results and Discussion

3.1. Characterization of BSA stabilized copper nanoclusters

BSA stabilized CuNCs were prepared based on the reduction of copper salts by BSA in the alkaline aqueous solution via the one-pot hydrothermal method. The amino acid residues which are cysteine, histidine, and tyrosine, in BSA play important and different roles to create the nanoclusters. The first two of these amino acids can coordinate with metal ions, while the last one can reduce metal ions to form metal NCs. The physical/chemical structure and optical features of prepared BSA-CuNCs were evaluated by using TEM analysis, zeta potential and dynamic light scattering

measurements, different spectroscopic techniques such as UV-vis, fluorescence spectroscopy, and XPS. The TEM image showed that the BSA-CuNCs were well-dispersed spherical shape with an average diameter of 2.1 nm particle size and distribution was uniform (not shown). Additionally, 3.6 nm particle size, the slightly larger size due to the hydrodynamic radius, was obtained from dynamic light scattering analysis which agreement with TEM analysis (Figure 1A). Moreover, obtained results from zeta potential analysis showed that synthesized BSA-CuNCs have a negative and high zeta potential value -31.5 mV in the working buffer solution (pH at around 12). This negative value represents synthesized nanoclusters have negatively charged and protected the copper nanoclusters from aggregation. The stability studies showed that synthesized nanoclusters were stable for at least 2 months without considerable precipitation in the refrigerator at 4°C .

In order to identify the changing of surface groups, the FT-IR spectra of BSA and BSA-CuNCs were recorded (Figure 1B). As shown from the figure, in BSA spectra, the three peaks corresponding to -NH bending (1530 cm^{-1}), -CN stretching vibrations (1230 cm^{-1}), and amine scissoring (1640 cm^{-1}) were observed. Moreover, the bending vibrations peak attributed to -OH group in carboxylic acids was observed at 1385 cm^{-1} . Similar peaks at 1598 cm^{-1} and 1300 cm^{-1} related to -NH bending and -CN stretching were observed in the BSA-CuNCs spectrum indicating interaction with CuNCs and BSA. Besides, -NH scissoring peak was disappeared which can be explained by the reaction of -NH group with copper during the formation of CuNCs. In addition to these results, although pure BSA has a peak at 280 nm, a weaker peak at 325 nm appears after synthesis of BSA-CuNCs, which can prove the formation of new material in the synthesized environment (Figure 2).

The XPS survey was introduced to explore the components of BSA stabilized CuNCs, and five major peaks at 162, 284, 398, 530, and 932 eV related to S 2p, C 1s, O 1s, N 1s, and Cu 2p were observed (Figure 1C).

In order to evaluate the spectroscopic character of the synthesized BSA stabilized CuNCs, UV-vis and fluorescence spectra were recorded. Absorption spectrum showed that (Figure 2) no plasmonic absorption peak was observed at the visible wavelengths. This result approves the absence of larger copper nanoclusters in synthesis media. To investigate the fluorescent properties of the synthesized BSA stabilized CuNCs, excitation and emission spectra were recorded and they showed a maximum emission peak at 405 nm when excited at 325 nm.

3.2. Optimization of CuNCs synthesis conditions

In this work, BSA was used as a stabilizer for the preparation of CuNCs. Cu^{2+} ions and BSA formed a complex through electrostatic binding and coordination interactions owing to functional groups of BSA such as $-\text{NH}_2$, $-\text{SH}$. The effect of reaction time, concentration of metal ion, and pH were examined to define the optimum synthesis conditions. In order to determine the effect of copper ion concentration, different volumes of copper ion solution were examined. As shown in Figure 3, the emission of clusters is dependent on various metal ion concentrations, and emission reduction occurs as nanoparticles are formed at higher metal ion concentrations. The second key parameter was pH to obtain a high concentration of BSA-CuNCs. For this purpose, phosphate buffer solutions with different pH values and NaOH solution were examined (Figure 4). Obtained results show that higher fluorescence emission intensity was

obtained for the reaction with 3.33 mM $\text{Cu}(\text{NO}_3)_2$ solution at pH 12 and this pH was selected. Another crucial step was the mixing time of nanoclusters which affected the fluorescence properties of BSA-CuNCs. Therefore, the effect of mixing time on the fluorescence emission intensity of BSA-CuNCs from 0 to 7.5 h was examined. As seen from Figure 5, the maximum intensity was obtained at 7th h. The emission signal of BSA-CuNCs decreased after this time, this may be due to overgrowth or aggregation. The experimental results proved this hypothesis because with the longer incubation time precipitation occurred and the color of BSA-CuNCs changed to dark brown.

3.3. The selections of experimental conditions

In order to identify optimum experimental conditions, the effect of different parameters such as pH and incubation time on the luminescence of BSA-CuNCs were examined. The obtained results showed that the fluorescence emission of BSA-CuNCs was pH-dependent. As seen from Figure 6A, at basic area high emission signal was achieved. This can be attributed to an increase of pair of electrons of BSA at basic pH, while at acidic medium the neutralization of negatively charged BSA-CuNCs was occurred due to high proton concentrations. Therefore, followed experiments were carried out at pH 12.

The effect of incubation time was also identified from 0 to 5 min and there was no difference in emission signal after 1 min. Hence, reaction time was chosen as 1 min as the experimental condition (Figure 6B). All optimization figures were given with error bars (Standard deviation, SD, and n=3).

3.4. Selectivity of Method

The selectivity of the nanoclusters for the detection of ORN was also evaluated. The effect of excipients such as propylene glycol and ethanol in injection form, starch and

magnesium stearate in tablets, and different ions such as K^+ , Na^+ , Mg^{2+} , Cl^- , SO_4^{2-} , CO_3^{2-} , and NO_3^- were tested under optimized experimental conditions. The fluorescence emission of the BSA-CuNCs was measured at 405 nm. The ORN concentration was 36 μM and excipients / metal ion concentration was 360 μM . As seen from the bar diagram of the fluorescence intensity change (Figure 7), only ORN showed a remarkable quenching of the BSA-CuNCs fluorescence, while the other interfering molecules and ions did not cause a significant response.

3.5. Fluorescence Quenching Mechanism

BSA stabilized CuNCs have excellent chemical and spectroscopic properties such as simple synthesis procedure, suitability to green chemistry, high and stable emission, low toxicity, hence in this study they were chosen to be the fluorescent probe for the determination of ORN in pharmaceutical formulations.

The change in the fluorescence spectra of BSA-CuNCs with successive additions of ORN were shown in Figure 8. It can be seen from the figure the fluorescence intensity of BSA-CuNCs was effectively quenched when the concentration of ORN increases, indicating an interaction between ORN and BSA-CuNCs. The previous study has also shown that the ORN has interacted with tyrosine residues of BSA molecules via hydrophobic and electrostatic forces [21].

Fluorescence quenching mechanisms can occur in several ways; static and dynamic (collisional) quenching, inner filter effect (IFE), and fluorescence resonance energy transfer (FRET). In static and dynamic processes, the fluorophore and the quencher should interact at the ground or excited state. In a static quenching system, both molecules compose a non-fluorescent molecule at the ground state, while in the

dynamic (collisional) quenching process, quenchers and fluorophores are interacting in the excited state. Both of them can cause non-radiative relaxation and decrease of fluorescence emission. The fluorescent resonance energy transfer (FRET) mechanism describes the energy transfer between two light-sensitive molecules, defined as donor and acceptor. For the IFE mechanism to occur, the absorption spectrum of the quencher and the excitation or emission spectrum of the donor must overlap. All these mechanisms can occur simultaneously and competitively.

Figure 2 shows the great overlapping between the absorption spectra of BSA-CuNCs and ORN. UV–Vis absorption spectra of BSA-CuNCs in the presence of ORN were also recorded and no observable variation was obtained. Moreover, it was noticed that there was a small part overlap between the emission band of CuNCs and the absorption peak of ORN, which may mean that the reabsorption of the NCs emission by ORN. According to Beer–Lambert Law, the molar absorption coefficient of ORN was calculated as 1.9×10^4 at 325 nm wavelength, which demonstrated that it was applicable to sensitive determination by IFE.

In addition, as seen from Figure 8, the fluorescence emission signal of BSA-CuNCs was quenched by adding ORN. Based on the above explanation, this decreasing in signal is due to the filtering effect. However, as mentioned earlier, other quenching mechanisms can also happen simultaneously. Stern-Volmer equation defines both static and dynamic quenching mechanism according to the following formula (Eq. 1) [23].

$$F_0 / F = 1 + K_{SV} [Q] \quad [1]$$

where F_0 and F indicate the fluorescence intensities of BSA-CuNCs before and after the interaction with ORN, respectively. K_{SV} is the Stern–Volmer quenching

constant and [Q] is the concentration of the ORN. K_{SV} is determined by the slope value of the linearity plot of the F₀/F and [Q].

A good linearity was obtained in the range from 2.35 to 61.70 μM with the regression coefficient of r = 0.9910 and equation F₀ / F = 0.02 [Q] + 0.92 (Figure 4 inset). The obtained results indicated that static quenching process occurred between the ORN and CuNCs system, and K_{SV} was calculated to be 1.96×10⁴ M⁻¹ which shows that interaction between drug and BSA-CuNCs is strong. These results showed that the synthesized nanoclusters can be applied as a fluorescent probe to determine ORN in pharmaceutical samples.

For better identification of the quenching mechanism, Eq. (2) was used to calculate the dynamic fluorescence quenching rate constant, K_q,

$$K_q = K_D / \tau_0 \quad [2]$$

where τ₀ is the average lifetime of the fluorophore in the absence of quencher and the value of τ₀ is 10⁻⁸ s for the biopolymer. For collisional quenching, the maximum scattering dynamic quenching constant of various quenchers is 2.0×10¹⁰ mol L⁻¹ s⁻¹. On the other hand, the K_q value was calculated as 1.96×10¹² mol L⁻¹ s⁻¹ which greater than the maximum dynamic quenching constant suggesting that there is a non-fluorescent complex is formed between the drug and nanoclusters [24]. This result confirms that the static quenching mechanism. The site binding model is used to define the number of binding sites (n) and binding constant (K) of ORN with BSA-CuNCs, Eq. (3).

$$\log ((F_0 / F) / F) = \log K + n \log [Q] \quad [3]$$

These values can be determined by the intercept and slope values of the regression plot of $\log(F_0-F)/F$ vs. $\log[Q]$. The n and K were found as 1.2 and $2.87 \times 10^5 \text{ M}^{-1}$, respectively. The high binding constant indicated a higher affinity between ORN and BSA-CuNCs. The binding constant (K) was also calculated with the Benesi-Hildebrand equation (4).

$$A_0/(A - A_0) = \epsilon_{\text{NCs}} / (\epsilon_{\text{ORN}} - \epsilon_{\text{NCs}}) + \epsilon_{\text{NCs}} / (\epsilon_{\text{ORN}} - \epsilon_{\text{NCs}}) \times 1/K [\text{ORN}] \quad (4)$$

where A_0 and A are the absorbance values of BSA-CuNCs before and after added of ORN, respectively. ϵ_{NCs} and ϵ_{ORN} are the molar absorption coefficients of BSA-CuNCs and its complex with ORN, respectively. In accordance with Eq. (4), the plot of $A_0/(A-A_0)$ against $1/[\text{ORN}]$ was constructed using the data from the spectrophotometric titrations and a linear fitting of the data yielded the binding constant (K) which was $3.04 \times 10^5 \text{ M}^{-1}$ for ORN-CuNCs. The binding constants obtained from fluorescence and UV-vis experiments were compatible.

The degree of repulsion between the similar charges present on the particle surface was described with Zeta potential and this force keeps from the aggregation and thereby increases the stability of particles. The measured zeta potential values of prepared particles were -31,5 mV and -15.8 mV in the absence and the presence of ORN, respectively, which might be indicated the aggregation of nanoparticles.

3.6. Detection of ORN in pharmaceutical forms

The proposed sensor was then applied for the quantitative analysis of ORN in pharmaceutical samples. The good linear correlation obtained using the sensor was achieved in the range of 0.52 to $13.56 \mu\text{g mL}^{-1}$ with an r value of 0.9934. The linear

regression equation was $F_0/F = 0.095 C (\mu\text{g mL}^{-1}) + 0.91$. The good linearity of the calibration graph and the negligible scatter of experimental points were evaluated by the values of the correlation coefficient and standard deviation values. Several approaches are given in the ICH guidelines to determine the limit of detection (LOD) and limit of quantification (LOQ). Limit of detection (LOD) and limit of quantification (LOQ) values were calculated according to the ICH guidelines by using equations $3 s/m$ and $10 s/m$, where s is the standard deviation of the response and m is the slope of calibration graph, respectively [25]. LOD and LOQ values were found as $0.01 \mu\text{g mL}^{-1}$ and $0.04 \mu\text{g mL}^{-1}$, respectively. In order to evaluate the repeatability and reproducibility of the proposed method, fluorescence intensities of five replicates were measured in the same (intraday precision) and following three days (inter-day precision). The values of inter- and intra-day precision were found 0.24 and 0.65, respectively. The results summarized in Table 1 indicate a high degree of precision for the proposed method. As indicated by the results (Table 1), the proposed method has a wide dynamic range, good accuracy, and a low detection limit. Hence, it allowed using quantitative determination of ORN in its pharmaceutical forms such as tablets and ampoules. Obtained results have good agreements with labeled values (Table 2). Recovery studies were performed in order to prove the accuracy of the proposed method, by adding samples with an appropriate amount of stock solution of ORN. The recovery values were in the range of 98.50–102.42 % (Table 2). These high recovery values proved the accuracy of the developed method. The proposed method has sensitivity and accuracy for determination from the pharmaceutical dosage forms. Our proposed approach was compared with other separation methods such as capillary electrophoresis [4], HPLC [5], and LC-MS [6], fluorescence [7, 21], and electrochemical techniques [8] for the determination of ORN

with respect to linear range, LOD, and recovery (Table 3). As seen from the table, the BSA–Cu NCs sensor has a wide linear range, high recovery, low detection limit value, and simplicity when compared with the previous studies. Thus, it holds great practicality for ORN detection in real pharmaceutical samples.

4. Conclusion

In this paper, the water-soluble fluorescent BSA-CuNCs were synthesized based on the reaction of copper ions and BSA in basic media by a one-pot hydrothermal process. The obtained results showed that fluorescence of BSA-CuNCs could be quenched due to the IFE mechanism between ORN and NCs. Synthesized and characterized nanoclusters were successfully applied as a fluorescence probe for the determination of ORN in pharmaceutical forms. High recovery values (98.50–102.42 %) with low RSD% values (0.25–2.73%) were achieved. The proposed method can be used as a promising tool for ORN analysis with its selective, selective, simple, rapid, and inexpensive properties.

References

1. Zhao L, Li J, Li Y, Wang T, Jin X et al. Preparation of monoclonal antibody and development of an indirect competitive enzyme-linked immunosorbent assay for ornidazole detection. *Food Chemistry* 2017; 229: 439-444. doi: 10.1016/j.foodchem.2017.02.100
2. Al Azzam KM, Saad B, Adnan R, Aboul-Enein HY. Enantioselective analysis of ofloxacin and ornidazole in pharmaceutical formulations by capillary electrophoresis using single chiral selector and computational calculation of

- their inclusion complexes. *Analytica Chimica Acta* 2010; 674 (2): 249-255. doi: 10.1016/j.aca.2010.06.046
3. Vaghani SS, Patel MM, Satish CS. Synthesis and characterization of pH-sensitive hydrogel composed of carboxymethyl chitosan for colon targeted delivery of ornidazole. *Carbohydrate Research* 2012; 347 (1): 76-82. doi: 10.1016/j.carres.2011.04.048
 4. See KL, Elbashir AA, Saad B, Ali ASM, Aboul-Enein HY. Simultaneous determination of ofloxacin and ornidazole in pharmaceutical preparations by capillary zone electrophoresis. *Biomedical Chromatography* 2009; 23: 1283-1290. doi: 10.1002/bmc.1251
 5. Wang Y, Zhang P, Jiang N, Gong X, Meng L, et al. Simultaneous quantification of metronidazole, tinidazole, ornidazole and morinidazole in human saliva. *Journal of Chromatography B* 2012; 899: 27-30. doi: 10.1016/j.jchromb.2012.04.032
 6. Du J, Ma Z, Zhang Y, Wang T, Chen X, et al. Enantioselective determination of ornidazole in human plasma by liquid chromatography–tandem mass spectrometry on a Chiral-AGP column. *Journal of Pharmaceutical and Biomedical Analysis* 2013; 86: 182-188. doi: 10.1016/j.jpba.2013.07.048
 7. Mehrzad-Samarin M, Faridbod F, Ganjali MR. A luminescence nanosensor for Ornidazole detection using graphene quantum dots entrapped in silica molecular imprinted polymer. *Spectrochimica Acta Part A: Molecular and Biomolecular Spectroscopy* 2019; 206: 430-436. doi: 10.1016/j.saa.2018.08.026
 8. Wang H, Bo X, Zhou M, Guo L. DUT-67 and tubular polypyrrole formed a cross-linked network for electrochemical detection of nitrofurazone and

- ornidazole. *Analytica Chimica Acta* 2020; 1109: 1-8. doi: 10.1016/j.aca.2020.03.002
9. Muñoz-Bustos C, Tirado-Guizar A, Paraguay-Delgado F, Pina-Luis G. Copper nanoclusters-coated BSA as a novel fluorescence sensor for sensitive and selective detection of mangiferin. *Sensors and Actuators B: Chemical* 2017; 244: 922-927. doi: 10.1016/j.snb.2017.01.071
 10. Aparna RS, Devi JA, Nebu J, Syamchand SS, George S. Rapid response of dopamine towards insitu synthesised copper nanocluster in presence of H₂O₂. *Journal of Photochemistry and Photobiology A: Chemistry* 2019; 379: 63-71. doi: 10.1016/j.jphotochem.2019.04.043
 11. Xu J, Zheng J. Quantum dots and nanoclusters. In: Genxi L (editors.). *Nano-inspired biosensors for protein assay with clinical applications*. Amsterdam, Elsevier. 2019, pp. 67-90
 12. Hu X, Liu X, Zhang X, Chai H, Huang Y. One-pot synthesis of the CuNCs/ZIF-8 nanocomposites for sensitively detecting H₂O₂ and screening of oxidase activity. *Biosensors and Bioelectronics* 2018; 105: 65-70. doi: 10.1016/j.bios.2018.01.019
 13. Pandit S, Kundu S. pH-Dependent reversible emission behaviour of lysozyme coated fluorescent copper nanoclusters. *Journal of Luminescence* 2020; 228: 117607. doi: 10.1016/j.jlumin.2020.117607
 14. Wang HB, Zhang HD, Chen Y, Ou LJ, Liu YM. Poly(thymine)-templated fluorescent copper nanoparticles for label-free detection of N-acetylcysteine in pharmaceutical samples. *Analytical Methods* 2015; 7 (15): 6372-6377. doi: 10.1039/C5AY00841G

15. Feng DQ, Zhu W, Liu G, Wang W. Dual-modal light scattering and fluorometric detection of lead ion by stimuli-responsive aggregation of BSA-stabilized copper nanoclusters. *RSC Advances* 2016; 6 (99): 96729-96734. doi: 10.1039/C6RA21470C
16. Guo Y, Shi S, Fan C, Jin D. Fluorescent determination of fluazinam with polyethyleneimine-capped copper nanoclusters. *Chemical Physics Letters* 2020; 754: 137748. doi: 10.1016/j.cplett.2020.137748
17. Zhao Z, Li Y. Developing fluorescent copper nanoclusters: Synthesis, properties, and applications. *Colloids and Surfaces B: Biointerfaces* 2020; 111244. doi: 10.1016/j.colsurfb.2020.111244
18. Yuan X, Luo Z, Yu Y, Yao Q, Xie J. Luminescent noble metal nanoclusters as an emerging optical probe for sensor development. *Chemistry An Asial Journal* 2013; 8 (5): 858-871. doi: 10.1002/asia.201201236
19. Park HJ, Shin DJ, Yu J. Categorization of quantum dots, clusters, nanoclusters, and nanodots. *Journal of Chemical Education* 2021; 98 (3): 703-709. doi: 10.1021/acs.jchemed.0c01403
20. Topală T, Bodoki A, Oprean L, Oprean R. Bovine serum albumin interactions with metal complexes. *Clujul Medical* 2014; 87 (4): 215. doi: 10.15386/cjmed-357
21. Ali HM, El-Hashemy MA. Analytical investigation of the influence of ornidazole on the native protein fluorescence. *Spectrochimica Acta Part A: Molecular and Biomolecular Spectroscopy* 2018; 201: 178-184. doi: 10.1016/j.saa.2018.05.003

22. Goswami N, Giri A, Bootharaju MS, Xavier PL, Pradeep T et al. Copper quantum clusters in protein matrix: potential sensor of Pb²⁺ ion. *Analytical Chemistry* 2011; 83(24): 9676-9680. doi: 10.1021/ac202610e
23. Lakowicz JR. (editors). *Principles of Fluorescence Spectroscopy*. Boston: Springer Science & Business Media, 2013.
24. Demirhan BE, Kara HEŞ, Demirhan B. One-step green aqueous synthesis of blue light emitting copper nanoclusters for quantitative determination of food color Ponceau 4R. *Journal of Photochemistry and Photobiology A: Chemistry* 2021; 417: 113356. doi: 10.1016/j.jphotochem.2021.113356
25. ICH Guideline (Q2A) (R1) Validation of analytical procedures: text and methodology IFPMA, Geneva, 2005.

Figure 1. (A) Dynamic light scattering result of BSA-CuNCs, (B) FT-IR spectrum of BSA (red line) and BSA-CuNCs (blue line), (C) The survey XPS spectrum of BSA-CuNCs.

Figure 2. UV-vis absorption (a) and fluorescence emission (b) spectra of BSA-CuNCs, absorption spectra of ORN (c) and BSA (d).

Figure 3. The effect of copper ion concentration on fluorescence emission of BSA-CuNCs. The final metal ion concentrations were 1.81 mM, 2.60 mM, 3.33 mM, and 4.61 mM at keeping BSA concentration same i.e., 15 mg/ml.

Figure 4. Photoluminescence spectra for BSA-CuNCs synthesized at different pHs (3-13)

Figure 5. Effect of mixing time on fluorescence emission of BSA-CuNCs.

Figure 6. Effect of pH and incubation time on fluorescence emission of BSA-CuNCs.

Figure 7. Effect of various interfering substances on the spectra (A) and the normalized $(F_0-F)/F_0$ of the system (B) (Concentration of ORN was 36 μM and interfering substances were 360 μM).

Figure 8. The effect of ORN concentration on fluorescence emission of the BSA-CuNCs. ORN concentration 2.35-61.70 μM in pH 12 phosphate buffer (from top to bottom, dotted line is QDs alone). The inset shows the change of the fluorescence intensity with the increase of the ORN concentration.

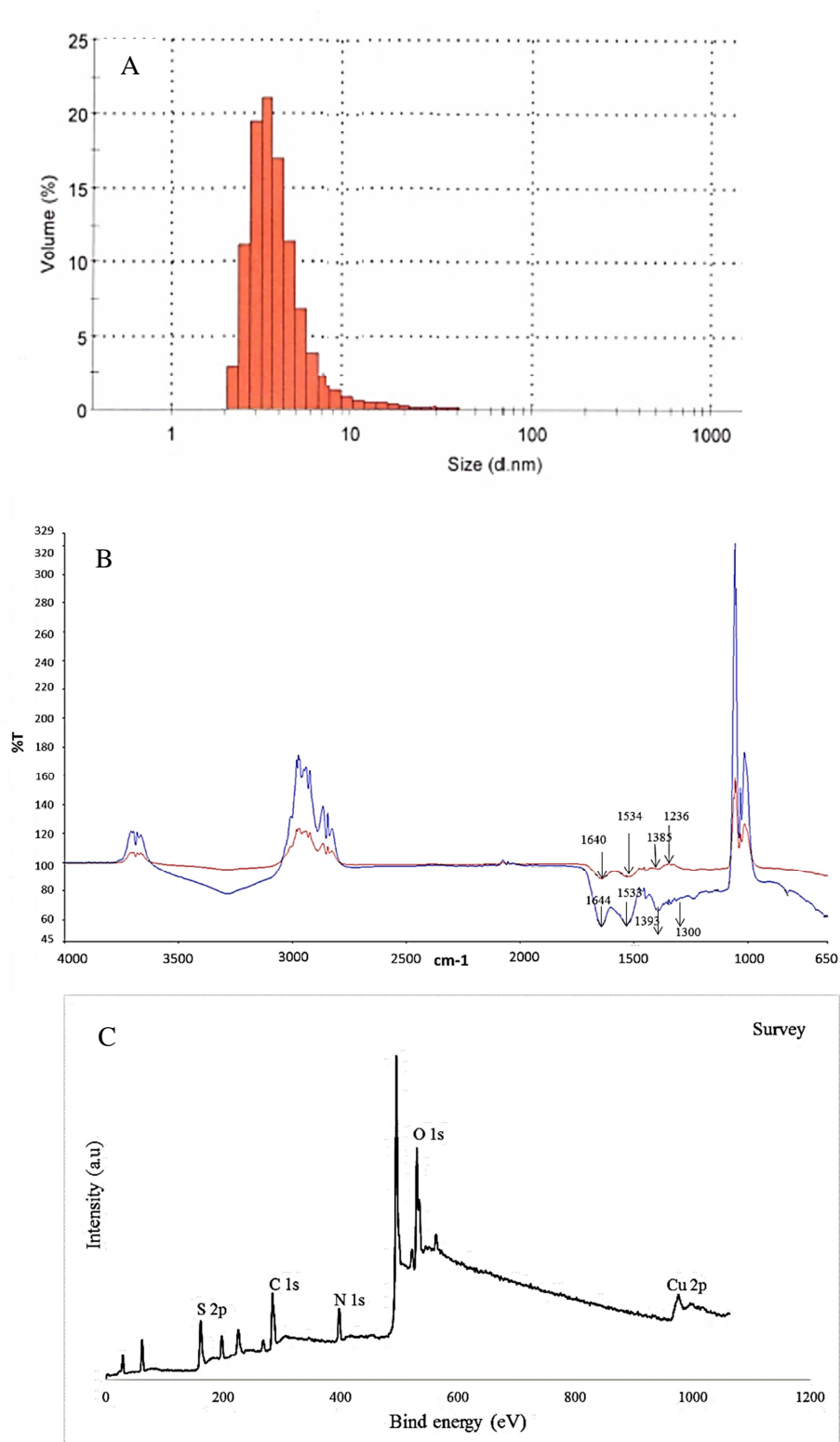


Figure 1. (A) Dynamic light scattering result of BSA-CuNCs, (B) FT-IR spectrum of BSA (red line) and BSA-CuNCs (blue line), (C) The survey XPS spectrum of BSA-

CuNCs.

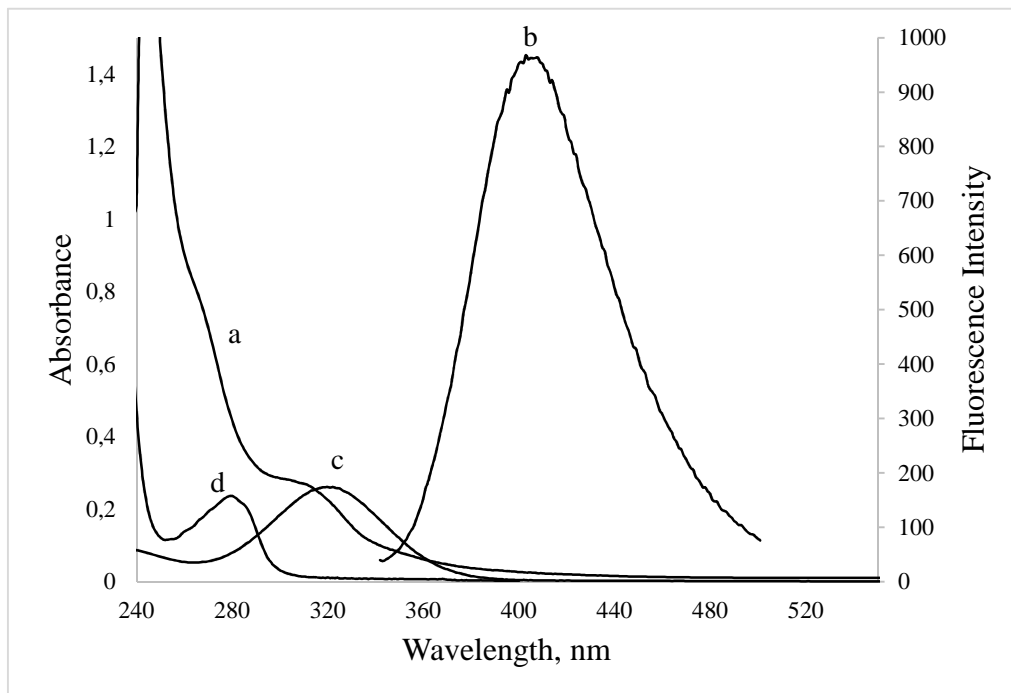


Figure 2. UV-vis absorption (a) and fluorescence emission (b) spectra of BSA-CuNCs, absorption spectra of ORN (c) and BSA (d).

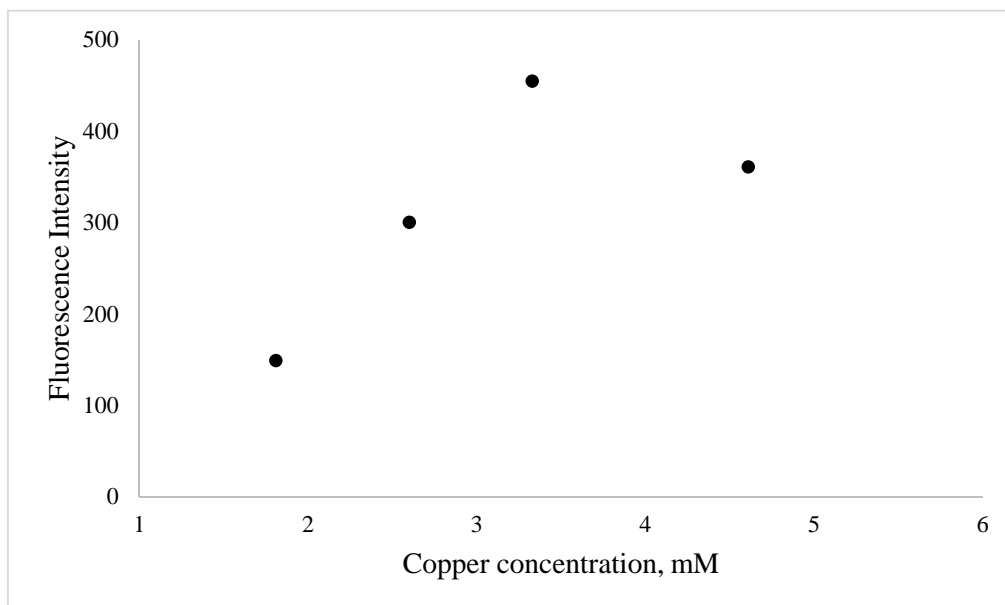


Figure 3. The effect of copper ion concentration on fluorescence emission of BSA-CuNCs. The final metal ion concentrations were 1.81 mM, 2.60 mM, 3.33 mM, and 4.61 mM at keeping BSA concentration same i.e., 15 mg/ml.

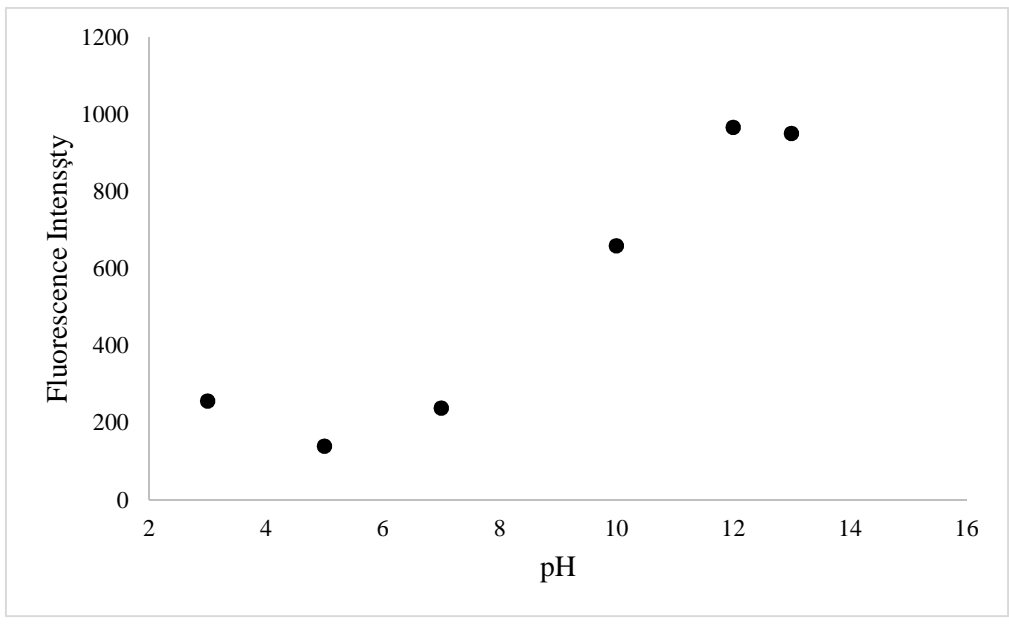


Figure 4. Photoluminescence spectra for BSA-CuNCs synthesized at different pHs (3-13)

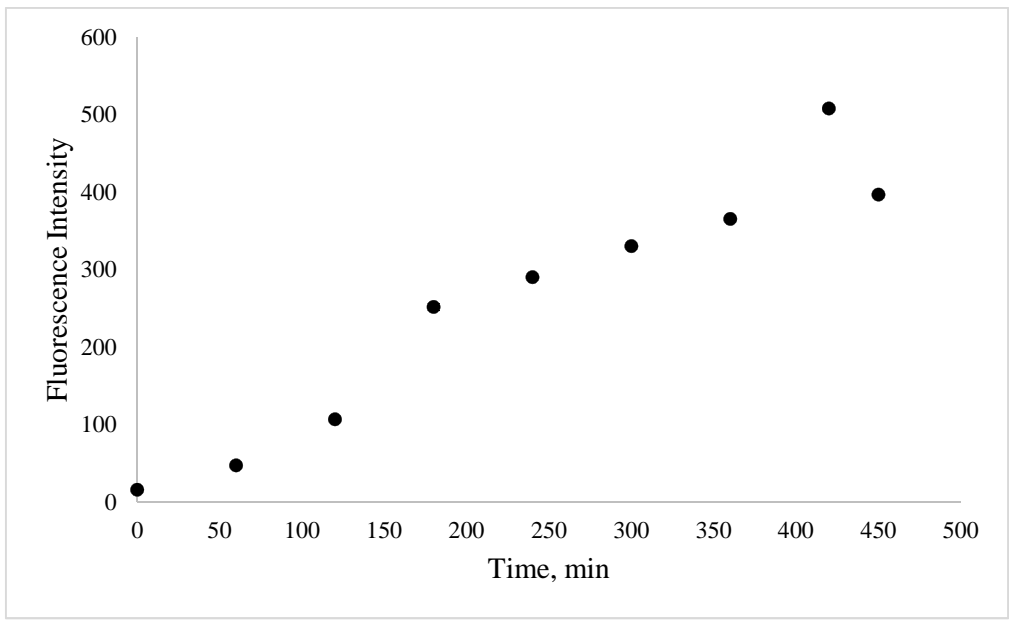


Figure 5. Effect of mixing time on fluorescence emission of BSA-CuNCs.

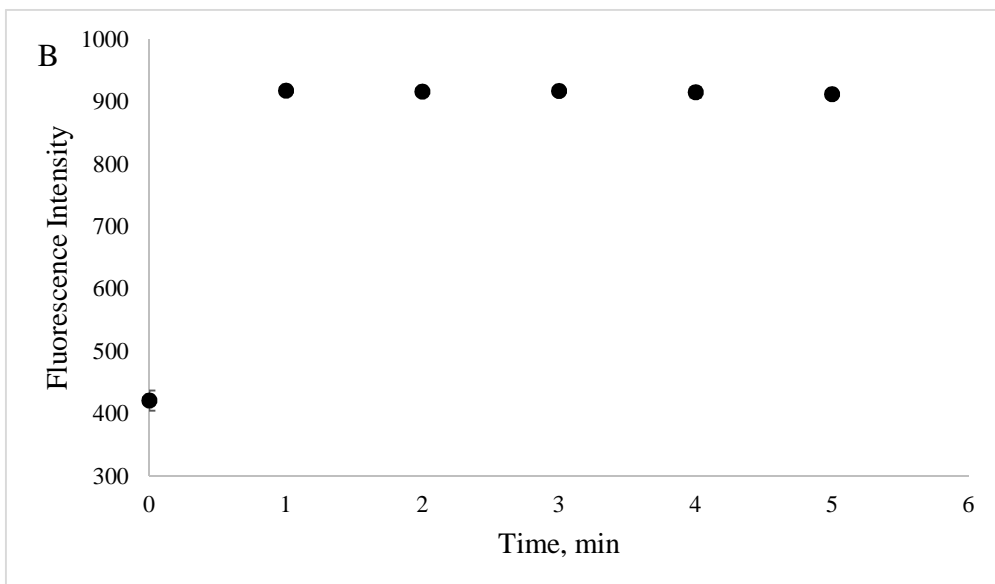
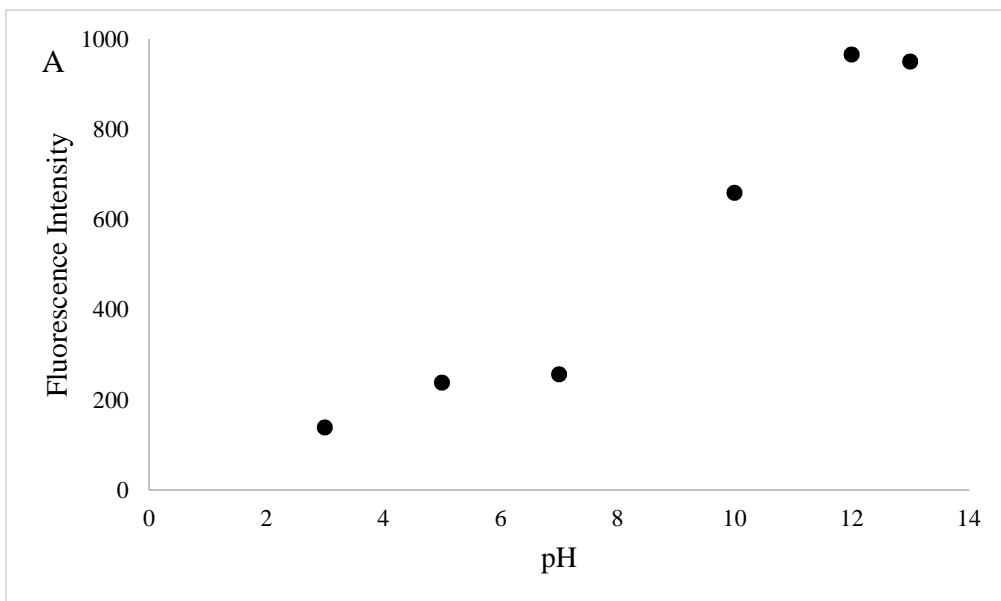


Figure 6. Effect of pH and incubation time on fluorescence emission of BSA-CuNCs.

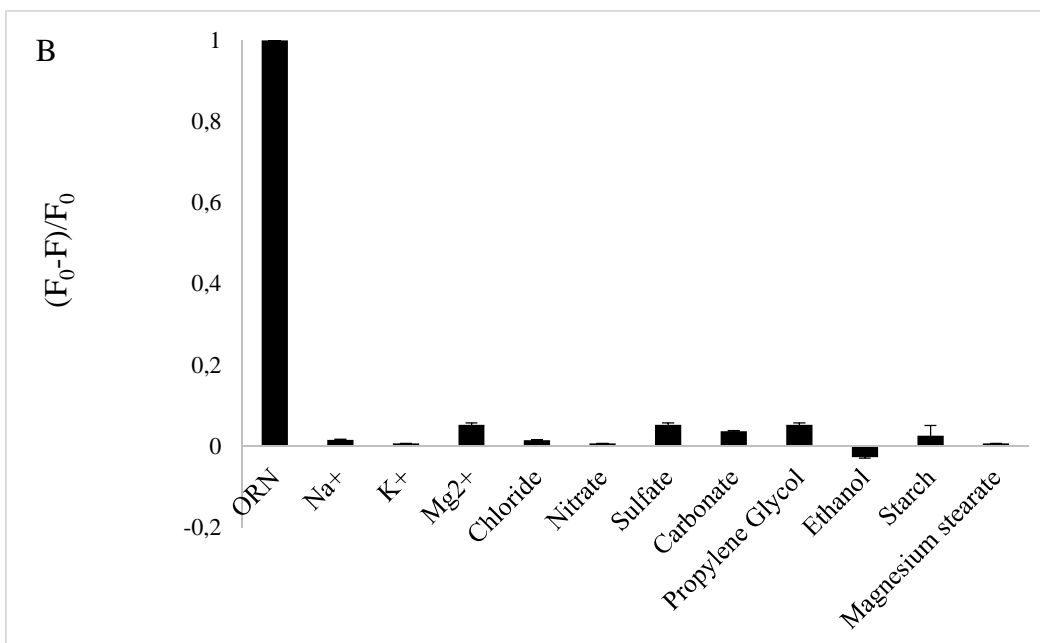
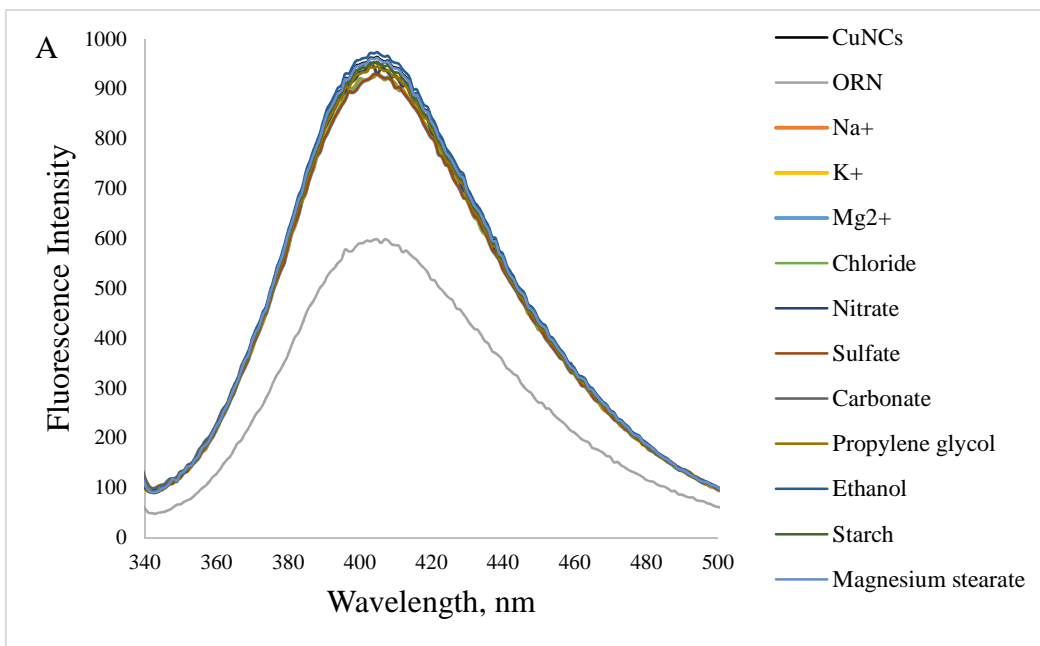


Figure 7. Effect of various interfering substances on the spectra (A) and the normalized $(F_0 - F) / F_0$ of the system (B) (Concentration of ORN was 36 μM and interfering substances were 360 μM).

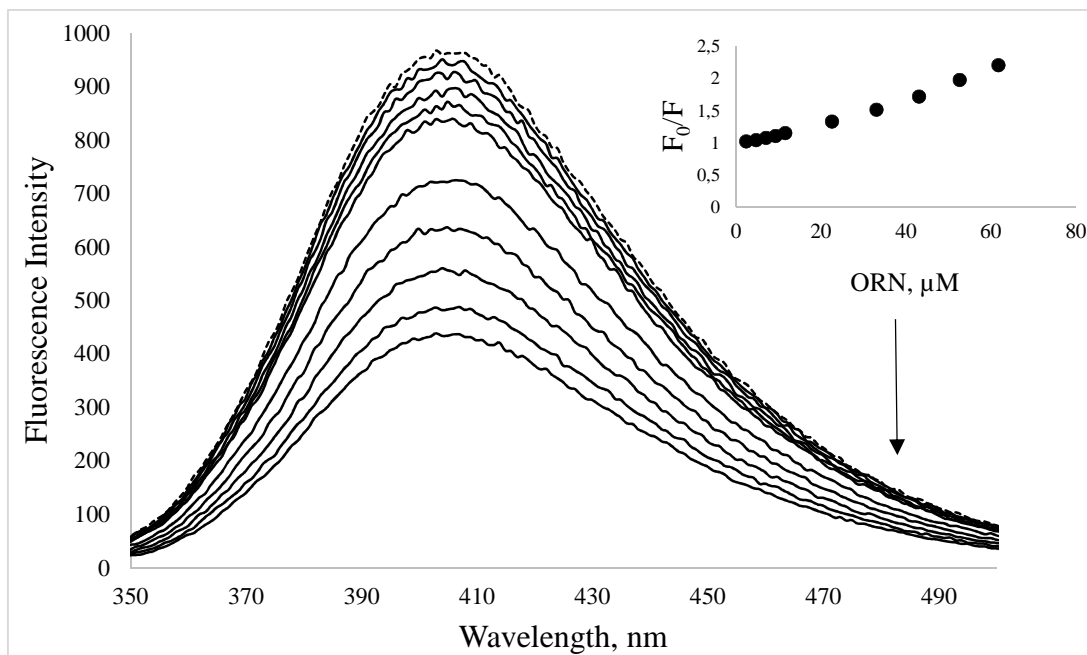


Figure 8. The effect of ORN concentration on fluorescence emission of the BSA-CuNCs. ORN concentration 2.35-61.70 μM in pH 12 phosphate buffer (from top to bottom, dotted line is QDs alone). The inset shows the change of the fluorescence intensity with the increase of the ORN concentration.

Table 1. Regression and validation parameters ORN by using BSA-CuNCs as a fluorescent probe

Linearity range ($\mu\text{g mL}^{-1}$)	0.52-13.56
Slope	0.095
Intercept	0.91
Correlation coefficient	0.9934
SE of slope	9.17×10^{-3}
SE of intercept	0.02
LOD ($\mu\text{g mL}^{-1}$)	0.01
LOQ ($\mu\text{g mL}^{-1}$)	0.04
Intra-day precision (RSD%)	0.24
Inter-day precision (RSD%)	0.65

SE: Standard error

RSD: Relative standard deviation

LOD: Limit of detection

LOQ: Limit of quantitation

Table 2. Dosage form and recovery analysis of ORN

Tablet (%)		Ampoule (%)	
99.70	Mean 99.04 RSD % 2.73	101.06	Mean 100.63 RSD % 0.25
103.40			
96.95			
95.51			
99.63			
100.24		100.56	
		100.64	
		100.64	
Added ($\mu\text{g mL}^{-1}$)	Found ($\mu\text{g mL}^{-1}$)	Recovery (%)	
1.65	1.69	102.42	
3.3	3.25	98.50	
4.95	4.90	99.00	

Table 3. Comparison of the proposed method with different techniques reported for the determination of ORN

Method	Linear range ($\mu\text{g mL}^{-1}$)	LOD ($\mu\text{g mL}^{-1}$)	Recovery (%)	Ref.
Capillary electrophoresis	25-250	1.80	96.2-105.2	4
HPLC	0.03–5.08	0.01	99.5–104.1	5
LC-MS	0.03–10.0	0.03	96.5-102	6
Fluorescence-Graphene QD	0.16-6.59	0.05	104.5	7
Electrochemical	0.15-22.1 22.1-54.9	0.05	99.3-100.4	8
Fluorescence	0.40-80	0.11	99.7-100.8	21
Fluorescence-BSA-CuNCs	0.52-13.56	0.01	98.5-102.4	This work